



Cite this: DOI: 10.1039/c7sm01132f

## Thermodynamic stability of worm-like micelle solutions†

Karsten Vogtt,<sup>a</sup> Gregory Beaucage,<sup>a</sup> Michael Weaver<sup>b</sup> and Hanqiu Jiang<sup>a</sup>

Worm-like micelles (WLMs) are nano-scale self-assemblies widely used for viscosity enhancement, for drug delivery, and in personal care products. The stability of WLMs under variable ionic and surfactant concentrations is important to applications of these fascinating materials. In this work it is demonstrated that a virial approach can be used to understand and predict WLM stability. A mixed surfactant system consisting of sodium laureth sulfate and cocoamidopropyl betaine was examined using small-angle neutron scattering. A linear relationship between the second virial coefficient,  $A_2$ , and the salt to surfactant ratio,  $\theta_{s-s}$ , is derived and demonstrated. The  $\theta_{s-s}$ -dependent term is described via association/dissociation kinetics of salt ions between the bulk and an ion cloud surrounding the WLMs yielding,

$$A_2 = \frac{b}{M^2} \left[ 1 - \left( \frac{n_{\text{surf}}}{K_{\text{eq}}} \right)^{\vartheta} (\theta_{s-s} - \theta_{s-s}^{a=0}) \right],$$

where  $K_{\text{eq}}$  is the association/dissociation constant,  $n_{\text{surf}}$  is the molar surfactant concentration,  $b$  is the molar excluded volume,  $M$  the WLM molar mass,  $\theta_{s-s}$  is the salt–surfactant ratio and  $\theta_{s-s}^{a=0}$  is the salt–surfactant ratio where the interactions are solely determined by the excluded volume. The ratio  $b/M^2$  is independent of WLM contour length. The exponent  $\vartheta$  is found to be approximately 5/4 in agreement with polymer scaling laws for the semi-dilute regime in good solvents.

Received 6th June 2017,  
Accepted 19th July 2017

DOI: 10.1039/c7sm01132f

rs.c.li/soft-matter-journal

## Introduction

Chain-like molecular assemblies or networks composed of nano-sized subunits can be found in technical products and biological matter. For example, the anionic or cationic surfactants in soap solutions can form worm-like micelles (WLMs), which govern visco-elastic properties.<sup>1,2</sup> In the life sciences, polymers and aggregates like DNA and fibrin<sup>3–5</sup> are prominent examples of tortuous or branched structures playing a pivotal functional role in biological systems. Important macroscopic properties like viscosity or rigidity are directly related to the microscopic structural parameters like the persistence length  $l_p$ , mesh size, and contour length  $L$ .

A convoluted WLM chain contains an average local concentration within the coil that can be calculated from the ratio of the coil mass and volume. This concentration is termed the overlap concentration,  $c_m^*$ , where  $c_m$  denotes the concentration in units of mass per volume. At solution concentrations above the overlap concentration, in the semi-diluted regime, there is a higher possibility of local mutual entrainment between WLMs, while below  $c_m^*$  the WLMs can be considered isolated in the

dilute regime at all size scales. At very high concentrations a concentrated regime is found where WLMs will display organization and correlation. (The concentrated regime can involve phase transitions and phase separation.) In the semi-dilute regime such ordering is not observed.

A distinguishing characteristic of the semi-dilute regime is that the thermodynamic properties of WLMs, such as the osmotic pressure, do not depend on the contour length.<sup>6–8</sup> Rather than the contour length, a new size, the mesh size,  $\xi$ ,<sup>9</sup> appears that reflects the average separation distance of the WLMs in an entrained network. In the dilute regime and at  $c_m^*$ ,  $\xi$  is identified with the WLM end-to-end distance which can, in turn, be related to the coil radius of gyration,  $R_{g,2}$  depending on the number of subunits,  $z$ , the mass fractal dimension,  $d_f$ , and chain topology. In the concentrated regime  $\xi$  is identified with the local cylinder diameter of the WLM. In the semi-dilute regime  $\xi$  scales with  $\xi \sim R(c_m/c_m^*)^{-3/4}$  for unbranched chains in a good solvent.<sup>9,10</sup>

In parallel to this static/thermodynamic structural model, rheology in the semi-dilute regime depends on dynamic features that have been related to structural models. When viscoelastic properties are first observed in increasing concentration, the entanglement concentration is reached,  $c_m^c$ . This concentration bears resemblance to  $c_m^*$  except that whereas  $c_m^*$  is a statistical concentration based on the size and mass of an average WLM, the entanglement concentration  $c_m^c$  depends on percolation of chain–chain interactions across the bulk sample. Since the

<sup>a</sup> Chemical and Materials Engineering, University of Cincinnati, Cincinnati, OH 45221, USA. E-mail: karsten.vogtt@uc.edu, beaucag@uc.edu

<sup>b</sup> P&G Analytical Sciences, 8700 Mason-Montgomery Rd, Mason, OH 45040, USA

† Electronic supplementary information (ESI) available. See DOI: 10.1039/c7sm01132f

interactions are time dependent  $c_m^e$  can have time dependence.  $c_m^e$  can also depend on the state of strain such as in extensional flow.<sup>11</sup> Due to these differences  $c_m^e$  and  $c_m^*$  may not agree. If a WLM solution displayed random clustering or fluctuations in WLM concentration the overlap concentration,  $c_m^*$  could be reached well before global percolation and  $c_m^e$ . Dynamics in the semi-dilute regime can depend on the contour length through the reptation theory of Edwards.<sup>12,13</sup> Rheology also depends on the entanglement distance,  $l_e$ , where  $l_e$  is the end-to-end distance between entanglements obtained from the plateau modulus.  $l_e$  appears closely related to  $\xi$ , though this could be misleading since one is a dynamic measure of the effective response of the network, while  $\xi$  is a static statistical measure. Again, the differences could be influenced by local clustering of concentration and by the shear rate. Both static and dynamic models for WLMs involve the unambiguous persistence or Kuhn length and the cylindrical diameter.

For large, coiled polymers the second virial coefficient,  $A_2$ , is indicative for interactions between the polymer subunits and the medium.  $A_2$  can be employed to calculate the Flory–Huggins interaction parameter  $\chi$ .<sup>14,15</sup> For WLMs it is known that their structure, in particular their length, changes with concentration. Due to this complication  $A_2$  will be directly considered in the framework of colloidal interactions following work with polyelectrolytes such as in protein and nucleic acid solutions rather than within the Flory–Huggins framework.

Studies of protein solutions have shown that  $A_2$  is a direct measure for the interactions between the molecules as well as a predictor for phase behavior such as crystallization or aggregation.<sup>16–19</sup> Positive values of  $A_2$  indicate net repulsive interactions and stable suspensions, negative values of  $A_2$  indicate unstable suspensions with attractive interactions between particles. For spherical particles such as lysozyme, relations have been elaborated, which describe the dependence of  $A_2$  and the pair-interaction potential between the dispersed particles.<sup>18</sup> For cylindrical geometries no such solutions are available. However,  $A_2$  might be qualitatively interpreted in the same manner as outlined above for WLMs. A positive  $A_2$  yields an osmotic pressure larger than for an ideal solution, which in turn can be intuitively attributed to prevalent repulsive forces between the WLMs. In the same manner a relationship can be drawn for a negative  $A_2$  and attractive forces.

The second virial coefficient is connected to the van der Waals parameters  $a$  and  $b$  via,

$$A_2 = \frac{1}{M^2} \left( b - \frac{a}{RT} \right) \quad (1)$$

where  $b$  represents the contribution of the excluded volume of the particles and  $a$  accounts for particle–particle interactions.<sup>10</sup>  $R$  when accompanied by  $T$  refers to the gas constant in this paper. In case that all Coulombic interactions are screened (Debye screening),  $a = 0$ , and  $A_2$  is solely determined by the (repulsive) contribution of the excluded volume  $b$ .<sup>15,16</sup>

$$A_2(a = 0) = \frac{b}{M^2} = \frac{V_{\text{ex}}^m}{M^2} = \frac{V^m f}{M^2} \quad (2)$$

where  $V_{\text{ex}}^m$  is the molar excluded volume,  $V^m$  is the molar volume and  $f$  is the ratio of excluded volume over particle volume, e.g.  $f = 4$  for hard spherical particles.

For long, stiff, rod-like particles with a length  $L$  and a radius  $R$  the following expression can be found<sup>20,21</sup>

$$f = \frac{L}{2R} + \frac{\pi + 3}{2} + \frac{\pi R}{2L} \quad (3)$$

For very long cylinders with  $L \gg 2R$ , eqn (3) simplifies to  $f \approx L/(2R)$ . Comparing eqn (2), bearing in mind that both the numerator  $V^m f$ , as well as the denominator  $M^2$  are proportional to  $L^2$  for WLMs, the dependence of  $A_2$  on  $L$  cancels. This means that, if  $a = 0$  and relation (3) holds for (flexible) WLMs,  $A_2$  adopts a constant value for all long, chainlike particles exhibiting the same radius  $R_1$  irrespective of their contour length  $L_2$ . This conclusion is supported by findings in polymer science, where it was found that for semi-diluted linear polymers the ratio of osmotic pressure  $\pi$  over  $c_m$  is independent of the molecular mass  $M \propto L_2$ .<sup>6</sup> The value of  $A_2$  should depend on Coulombic interactions in WLMs. The logical independent parameter is the salt to surfactant ratio,  $\Theta_{s-s}$ . As  $\Theta_{s-s}$  increases, saturation of the surface charge from the surfactant head groups should occur at  $\Theta_{s-s}^{a=0}$ . The examination of  $A_2$  at different salt–surfactant ratios,  $\Theta_{s-s}$ , should thus yield a constant value,  $A_2^{a=0}$ , where the values of  $A_2 = f(\Theta_{s-s})$  intersect. At this salt–surfactant ratio,  $\Theta_{s-s}^{a=0}$ ,  $A_2$  is solely governed by the excluded volume interactions i.e.  $A_2^{a=0} = b/M^2$  when  $a = 0$ .

### Measurement of $A_2$ for WLMs using small-angle neutron scattering

WLMs are disordered systems that can be described locally using a cylinder model. On large scales the structure can be quantified using a statistical approach. Here the mass distribution is expressed *via* the fractal dimensions  $d_{\text{min}}$ ,  $d_f$ , and  $c$ , where  $d_f$  is the mass fractal or extrinsic dimension and  $d_{\text{min}}$  is the fractal dimension describing the dependence of the minimum path length between two points at Pythagorean distance  $R$ .<sup>6</sup> The parameter  $c = d_f/d_{\text{min}}$  and is called the intrinsic or connectivity dimension.<sup>22–24</sup> This topological approach has been adapted in the form of a unified function describing the scattered intensity  $I(q)$  as function of momentum transfer  $q$  at small angle.<sup>25</sup> In a recent work we have complemented this unified function with a form factor  $P(q)$  for a cylinder to yield a hybrid function for  $I(q)$  of worm-like micelles.<sup>26</sup>

Employing the unified function, the scattered intensity  $I'(q)$  in the dilute regime can be expressed as the sum of two summands  $I_1(q)$  and  $I_2(q)$ , the first bearing the contribution of the building blocks of the structure and the latter containing the contribution of the overall or large scale structure.<sup>26</sup> The two terms are coupled following the unified approach<sup>25</sup> creating a hybrid scattering function.

$$I'(q) = I_1(q) + I_2(q) \quad (4)$$

Here  $I_1(q)$  refers to the scattering contribution of the cylindrical WLM-subunits, which is expressed through the form factor

for a cylinder.  $I_2(q)$  is formulated according to the unified function.<sup>24</sup>

At low concentration in the diluted regime this scattering function exhibits good agreement with experimental data. At higher concentrations, however, it is expected that spatial correlations between different WLMs will lead to a change at low  $q$ , *i.e.* at large correlation distances. If the WLMs exhibit a mutual preferential distance and orientation, one would expect to observe correlations or Bragg peaks. In semi-dilute solution, however, the WLMs will adapt more or less random orientations and at distances larger than the mesh size,<sup>9</sup>  $\xi$ , no structural information will be present. For the scattered intensity  $I(q)$  this means that at low  $q$ , below a minimum  $q^* \approx 2\pi/\xi$ , the scattered intensity becomes constant in  $q$ .

This behavior stems from structural screening.<sup>27</sup> One can compare this phenomenon with a fabric, where the observation from large distances corresponds to low  $q$ -values and inspection from short distances corresponds to large  $q$ -values. At a low yarn density (denier) or thread count, one will be able to identify a given thread at all spatial ranges. At high yarn densities and large overlap, however, one will be able to identify single threads and their cylindrical geometry from close distance, while viewing from large distances will yield the impression of a featureless tissue. At higher concentrations the screening size or mesh size becomes smaller.

The term “screening” is used with two distinct meanings for WLMs and these must be distinguished. The addition of salt leads to Debye screening of charge at size-scales larger than the Debye screening length,  $\lambda_D$ . Unfortunately, a similar term has been adopted for uncharged polymer chains to describe structural screening as discussed above. This structural screening can also be applied to polyelectrolytes and is applied in this paper to charged WLMs. To avoid confusion between electrostatic charge screening and structural screening (following the RPA equation discussed below), the former case is designated as Debye screening through out this paper.

In the present work scattering from surfactant WLMs in the semi-dilute regime is described using the random phase approximation (RPA). The WLM-system is formally treated with an analogy to semi-dilute polymers. The resulting thermodynamic parameterization differs from the polymer approach since chain contour length in WLMs depends on the systematic conditions. The second virial coefficient is used to describe thermodynamic stability.

At concentrations larger than  $c_m^*$ , the reduced scattered intensity  $I(q)/c_m$  exhibits a plateau-region at low  $q$ . With increasing number density of WLMs the mesh-size,  $\xi$ , will decrease, leading to a broadening of the plateau-region towards high  $q$  in inverse space. The transition between the plateau region and the local scattering observed at high- $q$  occurs at  $q \approx 2\pi/\xi$ . The random phase approximation (RPA) as adopted by de Gennes is used to describe this structural screening at low- $q$ .<sup>9,28</sup> In this paper, the formalism of Pedersen is followed,<sup>14,29–32</sup> eqn (5), which introduces the constant  $\nu$  having inverse units of intensity.  $\nu$  is proportional to the second virial coefficient,  $A_2$ , and the inverse of  $\nu$  is approximately given by the plateau intensity

at low- $q$  for WLMs in the semi-dilute regime.  $\nu$  depends on local interactions and has a temperature dependence following the dependence of  $A_2$ .

$$\frac{1}{I(q)} = \frac{1}{I_1(q) + I_2(q)} + \nu = \frac{1}{G_1(P_1(q) + (z-1)P_2(q))} + \nu \quad (5)$$

In eqn (5),  $G_1 = I_1(q=0)$  and  $z$  is the number of subunits or segments in the WLM so that for the dilute case, where  $\nu$  is much smaller than the first term,  $I(q=0) = G_1 + G_2$  and  $G_2/G_1 = z - 1$  (since  $I(q)$  is proportional to the concentration). The expressions  $P_1(q)$  and  $P_2(q)$  are the form factors of the respective contributions with  $P_i(q=0) = 1$ . In the case of WLMs, which exhibit a local cylindrical geometry,  $P_1(q)$  is given by a form factor for a cylinder.<sup>33</sup> For  $\nu \neq 0$  and for WLMs with many subunits in the semi-dilute regime, the first term on the right hand side of eqn (5) is approximately zero relative to  $\nu$ , so that  $I(q=0)^{-1} \approx \nu$ . Accordingly  $\nu$  can be determined *via* extrapolation of  $I(q \rightarrow 0)$  in the semi-dilute regime. The parameter  $\nu$  is related to the osmotic pressure through  $(d\pi/dc)^{-1}$  and can be expressed in the form of a virial expansion,<sup>14</sup>

$$\nu G_1 = 2A_2 M c_m + 3A_3 M c_m^2 + 4A_4 M c_m^3 + \dots \quad (6)$$

where  $M$  is the molecular mass and  $A_i$  depicts the respective virial coefficients. Note that virial coefficients are given with different units, *i.e.* different normalizations, in the literature. Throughout this work the concentration-normalized form bearing the units [mol ml g<sup>-2</sup>] is employed. Usually just the linear term of eqn (6) with the second virial coefficient  $A_2$  is taken into account and higher order terms are neglected, so that the RPA can be employed to determine  $A_2$  *via* light scattering:<sup>34</sup>

$$\frac{K c_m}{R_c(q=0)} = \frac{1}{M} + 2A_2 c_m \quad (7)$$

Here  $K$  is a system-specific constant and  $R_c(q)$  is the Rayleigh factor. Let  $M_{\text{cyl}}$  be the molar mass of a single cylindrical subunit so that  $z \times M_{\text{cyl}}$  is the molar mass  $M_{\text{WLM}}$  of the overall WLM. Then multiplying eqn (5) with  $G_1/M_{\text{cyl}}$  for  $q=0$  yields:

$$\frac{G_1}{M_{\text{cyl}} I(q=0)} = \frac{1}{M_{\text{WLM}}} + \frac{G_1}{M_{\text{cyl}}} \nu \quad (8)$$

Comparison of eqn (7) and (8) shows that

$$\nu \frac{G_1}{M_{\text{cyl}}} = 2A_2 \phi_m \quad (9)$$

Eqn (9) can be rewritten using,

$$\begin{aligned} G_1 &= \frac{N}{V_0} (\Delta\rho)^2 V_{\text{cyl}}^2 = \phi (\Delta\rho)^2 V_{\text{cyl}} \\ c_m &= \frac{N M_{\text{cyl}}}{V_0 N_A} \\ M_{\text{cyl}} &= \rho_{\text{cyl}} V_{\text{cyl}} N_A \end{aligned} \quad (10)$$

where  $N$  is the number of cylindrical subunits in the total sample volume  $V_0$ ,  $\phi$  is the volume fraction,  $N/V_0$  is the number density of cylinders,  $\Delta\rho$  is the scattering length density difference between the WLM and the solvent,  $\rho_{\text{cyl}}$  is the mass density

and  $V_{\text{cyl}}$  is the volume of the cylindrical subunit. Substitution of relations (10) into eqn (9) yields,

$$\nu = 2A_2N_A \left( \frac{\rho_{\text{cyl}}}{\Delta\rho} \right)^2 \quad (11)$$

The parameter  $\nu$ , as defined in eqn (5) is thus independent of concentration, which can be easily shown through normalization of  $\nu$  to  $G_1$ ,

$$\nu = \frac{\nu_0}{G_1}, \quad (12)$$

yielding the dimensionless parameter  $\nu_0$  (see eqn (6)). Now eqn (5) and (11) can be rewritten

$$I(q) = G_1 \frac{P(q)}{1 + \nu_0 P(q)} \quad (13)$$

$$\nu_0 = 2A_2\rho_{\text{cyl}}^2 V_{\text{cyl}}^{\text{m}} \phi, \quad (14)$$

defining the molar volume of a cylindrical subunit  $V_{\text{cyl}}^{\text{m}} = N_A V_{\text{cyl}}$ , where  $N_A$  is Avagadro's number.

Eqn (13) represents a very common mathematical form to define  $I(q)$  in semi-dilute systems.<sup>14,35</sup> Bearing in mind that a density times the according molar volume yields the molar mass, eqn (14) is identical with the linear part of relation (6). Since  $\nu_0$  as well as  $G_1$  are proportional to concentration, the according dependence of  $\nu$  as the ratio of these two values cancels out.

## Materials and methods

Chemical compounds and rheological characterization were as described in ref. 26. A mixed surfactant was used consisting of sodium laureth-1 sulfate and cocoamidopropyl betaine (molar mixing ratio 9:1). A concentration series between 0.232 and 3.72 wt% of mixed surfactant were studied. To probe the impact of salt and electrostatic screening,  $I(q)$  was determined at various salt concentrations (3.01, 3.56, 4.01, 4.5 and 5.0 wt% NaCl).

Flow viscosity measurements were made either using a TA Instruments DHR3 rheometer with cup and bob geometry or an Anton Paar Lovis ME2000 rolling ball viscometer. For DHR3, the temperature was controlled using a Peltier cup accessory and a solvent trap was used to maintain the environmental integrity. The viscosity flow curves were collected using TRIOS software using steady-state sensing, and the zero shear viscosity was verified by measuring over several shear rate settings below  $0.1 \text{ s}^{-1}$  to verify the zero-shear viscosity plateau at shear rates below the onset of the shear-thinning region. The reported zero shear viscosity was typically the average of several viscosity data points between 0.001 and  $0.01 \text{ s}^{-1}$ .

SANS-measurements were performed at Oak Ridge National Laboratory using the instruments Bio-SANS (High Flux Isotope Reactor, HFIR) and the EQ-SANS (Spallation Neutron Source, SNS). Data reduction and background subtraction were performed employing software provided by the beam line scientists. The EQ-SANS instrument employs the time-of-flight technique and exhibits superior resolution at high  $q$ -values. The SANS data was merged

from the Bio-SANS instrument (from about 0.001 to about  $0.07 \text{ \AA}^{-1}$ ) at low and intermediate  $q$  and from EQ-SANS at high  $q$  (above  $0.07 \text{ \AA}^{-1}$ ). The absolute intensities  $I(q)$  of the two instruments agreed within the instrumental accuracies in the respective  $q$ -regime. A small constant background associated with diffraction from the WLM structures was subtracted affecting the highest  $q$  values.

For mixed surfactant concentrations between 0.232 and 1.86% surfactant, no plateau regime in  $I(q)$  was found at the lower  $q$ -limit, especially at high NaCl concentrations. For a fit according to eqn (4) it is beneficial to have the complete Guinier regime of  $I_2(q)$ . Moreover for the extrapolation  $I(q \rightarrow 0)$  for the determination of  $\nu$  according to eqn (5), this plateau at low  $q$  is required (see Fig. S1 of the ESI†). Therefore static light scattering (SLS) experiments were undertaken to evaluate the trend of  $I(q)$  at  $q$ -values below  $0.002 \text{ \AA}^{-1}$ . SLS measurements were performed using a pinhole detector equipped in a Brookhaven BI-200SM goniometer to collect scattered signal. The light source was a Coherent INNOVA (Coherent Verdi V10) argon laser ( $\lambda = 532 \text{ nm}$ ), (100–200 mW). Measurements were made through step scan with scattering angle from  $5^\circ$  to  $50^\circ$  at room temperature. The Brookhaven “SLS” software was used for data acquisition and Igor was employed for background subtraction. SLS data was scaled to match the SANS data with absolute intensity. (This instrument was kindly provided by Matt Lynch at Procter & Gamble's Winton Hill Facility.)

The fitting of the SANS/SLS data under diluted conditions followed the approach given in ref. 26. The WLMs were structurally characterized by size of their cylindrical subunits (subscript 1) as well as by the dimensions of the overall WLM (subscript 2).  $L_1$  represents the length of the cylindrical subunits, while the radius was modeled with a polydisperse distribution using a lognormal distribution with median value  $R_1$  and the geometric standard deviation, a dimensionless width parameter,  $\sigma_{R_1}$ . The volume fraction  $\phi$  as well as the scattering length densities of the WLMs  $\rho_{\text{W}}$  and of the solvent  $\rho_{\text{s}}$  were combined to the factor  $\phi_{\text{v}}(\Delta\rho)^2$ , where  $\Delta\rho$  is the scattering length density contrast  $\rho_{\text{W}} - \rho_{\text{s}}$ . For the WLM coil made up of these rod subunits, the scattered intensity at zero angle  $G_2$ , the radius of gyration  $R_{\text{g},2}$  and the fractal dimension  $d_{\text{f},2}$  were obtained from the fits (see Introduction). For connectivity dimension  $c = d_{\text{f},2}/d_{\text{min},2}$  of the WLMs, the latter value  $d_{\text{min},2}$  was set to 5/3 assuming a self-avoiding walk for the subunits.<sup>24</sup> From all these parameters the number of subunits  $z$  and the branch content  $n_{\text{br}}$  of the WLMs can be calculated.<sup>26,36</sup>

At high surfactant concentrations, when the weight fraction normalized scattered intensity  $I(q)\phi^{-1}$  exhibited a flattening at low  $q$  as compared to the lowest concentration examined, eqn (5) was employed as a fitting function, including the structural screening parameter  $\nu$  in the double reciprocal form of eqn (4) according to the RPA formalism.

## Results

### Structural screening effect, large-scale structure and rheological properties

The weight-fraction-normalized scattered intensity  $I(q)/\phi_{\text{w}}$  for a concentration series of mixed surfactant in  $\text{D}_2\text{O}$  (5.0% NaCl) are

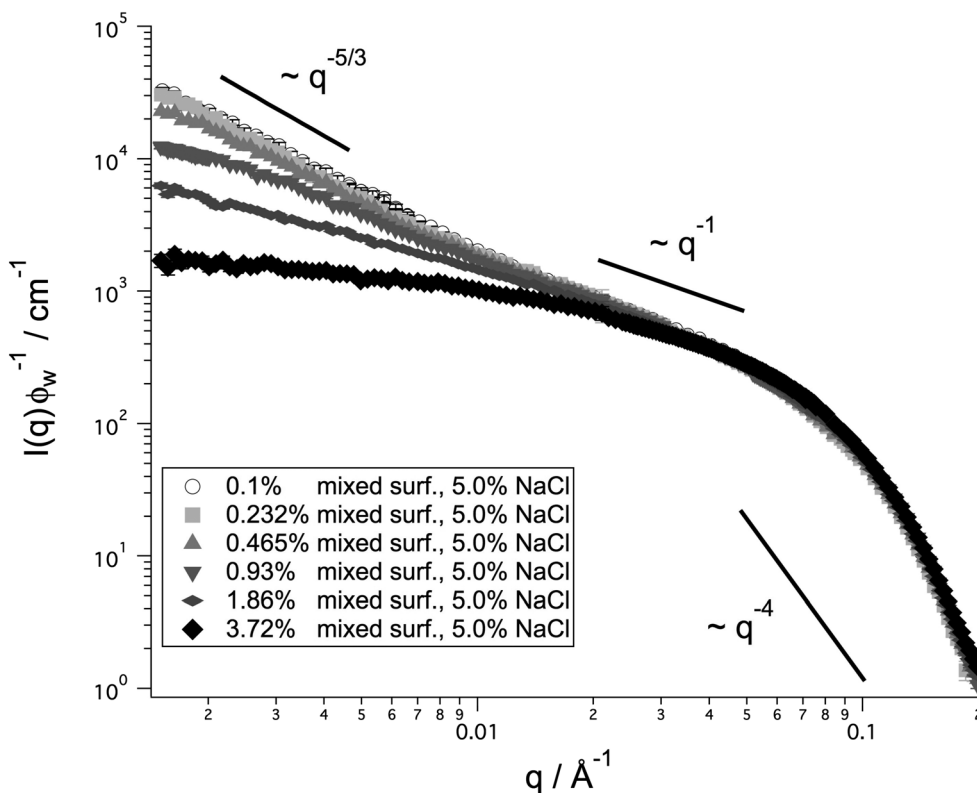


Fig. 1 Scattered intensity  $I(q)$  normalized by the weight percentage  $\phi_w$  for various concentrations of the mixed surfactant in presence of 5.0% NaCl.

shown in Fig. 1. While the curves agree well at high  $q$ , at low  $q$  a trend of flattening is clearly visible with increasing concentration. We attribute this behavior to the “screening effect” mentioned above. The normalized  $I(q)$  for the two lowest concentrations agree well, and besides the domain scaling with  $q^{-1}$ , indicative for elongated or rod-like objects in the respective spatial range, at lowest  $q$  a component scaling with roughly  $q^{-5/3}$  can be clearly identified. The latter can be attributed to the scattering contribution  $I_2(q)$  according to eqn (4), while the regimes scaling with  $q^{-1}$  and  $q^{-4}$  are represented by  $I_1(q)$ , the scattering contribution of the cylindrical WLM subunits. Accordingly the scattered intensity at 0.1 and 0.232 wt% of mixed surfactant can be considered free of interactions and can be fitted with eqn (4). Already at concentrations as low as 0.465 wt%, slight screening can be observed, which increases with increasing surfactant concentration.

For 0.93, 1.86 and 3.72 wt% mixed surfactant, the scattered intensity at low  $q$  flattens out with increasing concentration. For 0.93% mixed surfactant  $I_2(q)$  is affected, while at 3.72% of surfactant even the domain characterized by the  $q^{-1}$ -power law is basically flattened out. The concentrations from 0.465 to 3.72 wt% mixed surfactant were therefore fitted using eqn (5).

Fig. 2 shows the specific viscosity  $\eta_{sp}$  plotted against salt weight fraction (A) and the surfactant (B). Three factors increase the specific viscosity of a WLM system. On the one hand the contour length  $L_2$  governs  $\eta_{sp}$  in the diluted regime. Secondly, beyond  $c_m^e$ , entanglements lead to a further increase of the viscosity. Finally, at very high surfactant and/or salt concentrations, the onset of branching can lead to a decrease

of the viscosity.<sup>1</sup> All of these effects can be seen in Fig. 2 and they can be compared with the SANS analysis (see Fig. 1).

In the first step the cases where just  $L_2$  governs  $\eta_{sp}$  are identified. At 0.232% mixed surfactant, the specific viscosity  $\eta_{sp}$  increases monotonically with increasing salt concentration (Fig. 2A). This is in accordance with the trend of  $L_2$  observed by SANS (see Tables S1 and S2 in the ESI†) that indicates dilute conditions and Rouse behavior, Fig. 2, 0.232%. At 0.93% mixed surfactant  $\eta_{sp}$  increases initially, but runs into a plateau at about 4.5% NaCl in Fig. 2A. Fig. 1 shows this sample to be above the overlap concentration at 5% NaCl where the plateau in Fig. 2A occurs. A plausible explanation for this behavior is, that at this surfactant concentration the WLMs are entangled and that around 4.5% NaCl the onset of branching counteracts a further increase of  $\eta_{sp}$ . Thus it seems plausible to consider 0.232% mixed surfactant as dilute, while 0.465% marks the transition into the semi-diluted, overlapped regime. This impression is confirmed by the trend of  $\eta_{sp}$  vs.  $\phi_{w,NaCl}$  for 1.86 and 3.72% mixed surfactant. For the former sample the plateau is already observed at about 4% NaCl, at 5% salt  $\eta_{sp}$  even decreases. The effect is even more pronounced for 3.72% surfactant. In these two latter cases a further increase of  $\eta_{sp}$  via elongation of  $L_2$  and increase of entanglement is compensated for or overcome by branching.

A more concise and quantitative picture of these considerations can be gained by looking at the changes of  $\eta_{sp}$  with increasing surfactant concentration (Fig. 2B). For 3.01% NaCl two power law regimes can be identified. The first spans from 0.232 to about 0.93% mixed surfactant, exhibiting a power law

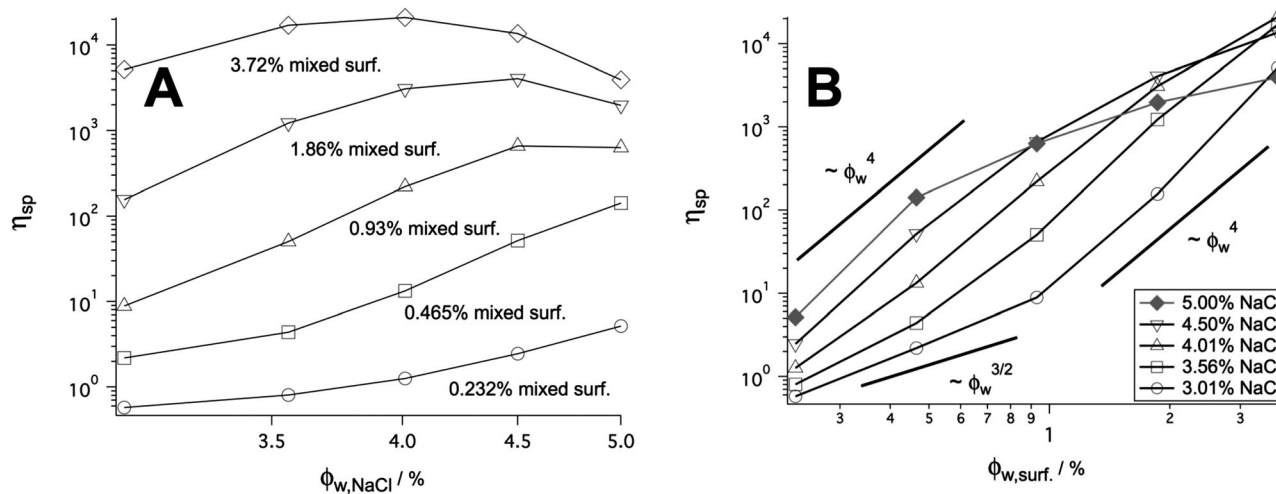


Fig. 2 Log–log plot of the specific viscosity,  $\eta_{sp}$ , vs. weight fraction NaCl (A) and log–log plot of  $\eta_{sp}$  vs. the mixed surfactant weight fraction (B). Connecting lines between the data points are a guide for the eyes, only.

of 3/2. The second regime with an exponent of about 4 is found between 0.93 and 3.72% of surfactant. According to the above considerations the regime with an exponent of 3/2 can be assigned to an increase of  $\eta_{sp}$  due to an elongation of  $L_2$ , while the increase with an exponent of 4 indicates an increase of  $\eta_{sp}$  due to elongation plus entanglement.

Addition of NaCl induces an increase of  $L_2$  and concomitantly a higher propensity for entanglement. Accordingly the power-law regime with the exponent 4 broadens upon addition of further NaCl (3.56%, see Fig. 2B). At 4% NaCl almost for the whole surfactant concentration range an increase of  $\eta_{sp}$  with a power law of 4 is observed, *i.e.* the WLMs between 0.232 and 3.72% mixed surfactant are in an entangled state.

At 4.5 wt% NaCl the scenario changes. At high surfactant concentrations a new power law regime appears, exhibiting an exponent below 4. Further addition of salt (5 wt%, see Fig. 2B) leads to a further decrease of the exponent and a broadening of the power law regime towards lower surfactant concentration. This new regime can be explained *via* the occurrence of branching, which counteracts the increase of  $\eta_{sp}$  caused by WLM elongation and entanglement.

Carefully bearing in mind that the SANS-data was collected under static conditions, while the rheological data was determined under mechanical shear, one can employ the occurrence of screening in  $I(q)$  as an indicator for overlap. However, the presence of screening expressed *via*  $\nu \neq 0$  impedes the assessment of the large-scale structure represented by  $I_2(q)$ . A thorough analysis of the information, which can be extracted in the different scattering scenarios, is given in the following section.

### SANS data and fitting results

Fig. 3 depicts the scattered intensity  $I(q)$  and a fit according to eqn (4) for 0.232 wt% mixed surfactant in presence of 3.01 wt% NaCl. The results of the fitting procedure as well as further values calculated from these results are depicted in Tables S1 and S2 in the ESI† It has to be noted that the values for the number of subunits  $z$  given in ref. 26 for 0.232 wt% of mixed

surfactant were too large by a factor of about 6 due to an error in an integration algorithm. However, the trends and conclusions reported in that publication are unaffected. The results presented in Table S1 of the ESI† report the corrected values based on the most recent data.

For 0.232 and 0.465 wt% the data allowed the large-scale parameters of the WLMs to be obtained (see Tables S1 and S2 in the ESI†). At low salt concentrations the data just could be fitted assuming linear WLMs (*i.e.* setting  $d_{\min,2} = 1.67$  and connectivity dimension  $c = 1$ ), with increasing salt concentrations connectivity dimensions  $>1$  are obtained indicating branching. Despite large error bars, a clear trend towards branching around 4.5 wt% NaCl is visible, in agreement with rheological findings (see Fig. 2 and according text). Most values of the branch content  $n_{br}$  are well below 1. This means there are generally less than one branch per WLM.

For concentrations of 0.93 and 3.72 wt% mixed surfactant, the large-scale structure could not be determined. For 0.93 wt% the large-scale parameters  $G_2$  and  $R_{g,2}$  were fitted just to obtain stable fits. The error bars for these values are all close to or larger than 100%. Just the structure of the cylindrical subunits could be determined for this sample set. The values for  $R_1$  and  $L_1$  are very similar for the whole range of surfactant concentrations, yielding values between 17–18 Å for the median radius and between 1100 and 1300 Å for the length of the cylinders.

For a concentration of 1.86% of mixed surfactant no stable, unambiguous fits were obtained. In order to obtain a stable fit, the contribution of  $I_2(q)$  has to be taken into account, because the approximation of  $I_2(q) \approx 0$  did not yield conclusive results. So just the  $\nu$  parameter could be extracted from the 1.86% data (see next section). The high  $q$ -region of the normalized scattered intensity  $I(q)$  for the 1.86% samples agrees well with the data from the other concentrations (see Fig. 1). Hence,  $R_1$  can be estimated to be within a range of 17–18 Å as found for the other samples.

At a surfactant concentration of 3.72% the ansatz  $I_2(q) \approx 0$  yielded stable fits.  $L_1$  was found to be a bit larger than for the lower surfactant concentrations and varies just slightly with salt

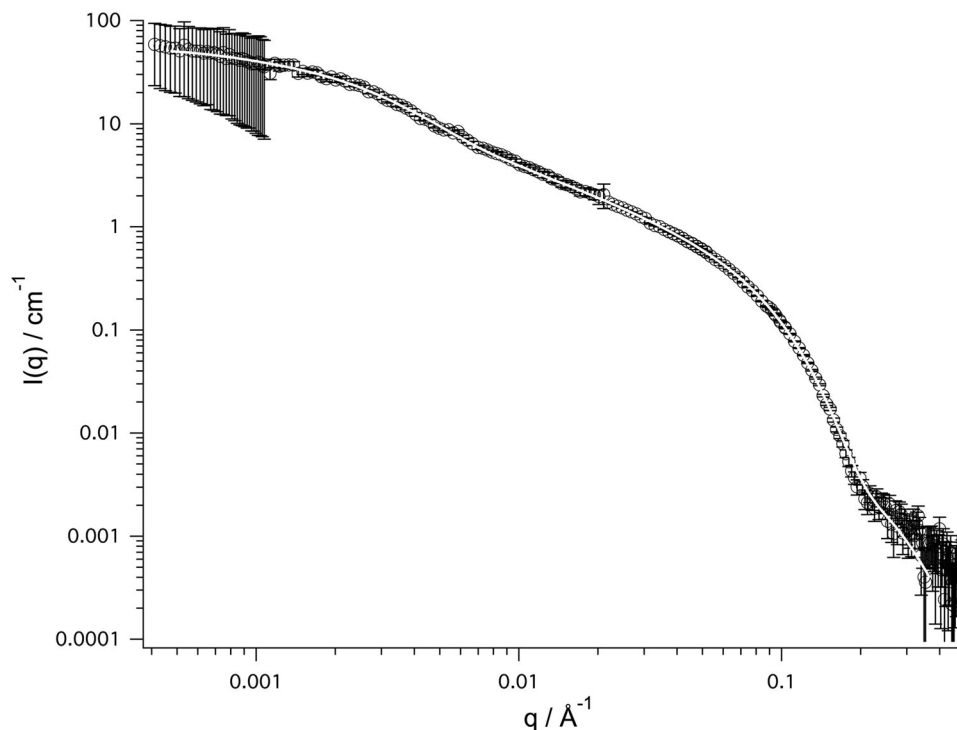


**Fig. 3** Double logarithmic plot of the SLS/SANS intensities  $I(q)$  for 0.232 wt% mixed surfactant in the presence of 3.01 wt% NaCl (black) and fit (white). The fit at high- $q$ , above  $0.15 \text{ \AA}^{-1}$ , is poor due to the complexity of the actual WLM structure compared to the simple cylindrical model with uniform scattering density. A more complex model would involve, at a minimum, 3 further parameters, which are not warranted by the data. The relatively large error bars at low- $q$  are for SLS data points where the signal is much weaker compared to SANS.

concentration. But all in all the structure of the cylindrical subunits hardly change with salt and surfactant concentration. SANS is sensitive to hydrogen contrast so the counter ions are seen only weakly and the observed radius is primarily that of the hydrophobic tails.

### The screening parameter $\nu$

Fig. 4 depicts  $\nu$  vs. the salt-surfactant ratio  $\Theta_{s-s}$ .  $\nu$  and  $A_2$  decrease with increasing  $\Theta_{s-s}$ , indicating reduced solubility of the WLMs at higher salt concentration. The interactions between micelles are mainly of electrostatic nature and increased salt concentration reduces the effective surface charge for the WLMs *via* Debye screening.

Fig. 4 shows that  $\nu$  follows approximately a linear relationship with the salt-surfactant ratio, dashed lines  $f(\Theta_{s-s})$ . The slopes ( $\Delta\nu/\Delta\Theta_{s-s}$ ) are 0.00310, 0.00115, 0.00053 and 0.00023 cm for 3.72, 1.86, 0.93 and 0.465 wt% of mixed surfactant. All the lines cross at one point  $\nu \approx 0.0185 \text{ cm}$  and  $\Theta_{s-s} \approx 6.16$ , referred to as  $\nu^{a=0}$  and  $\Theta_{s-s}^{a=0}$ . The inset of Fig. 4 shows a double logarithmic plot of  $(\Delta\nu/\Delta\Theta_{s-s})$  vs. the molar surfactant concentration  $n_{\text{surf}}$ . The values of  $(\Delta\nu/\Delta\Theta_{s-s})$  are connected to the surfactant concentration *via* a power law of about 5/4. Thus, the values of  $\nu$  as a function of  $\Theta_{s-s}$  can be expressed *via* a linear relationship,

$$\nu = \nu^{a=0} \left[ 1 - \left( \frac{n_{\text{surf}}}{K_{\text{eq}}} \right)^{\vartheta} (\Theta_{s-s} - \Theta_{s-s}^{a=0}) \right] \quad (15)$$

where  $K_{\text{eq}}$  is a constant in units of  $\text{mol l}^{-1}$  and  $\vartheta \approx 5/4$ . The change from the volume or weight fraction  $\phi$ , employed previously, to molar concentrations  $n$  as well as the choice of  $K_{\text{eq}}$  in eqn (15) is done in forethought to the next section of this paper, where a derivation of eqn (15) is given.

Since  $\nu$  is proportional to the second virial coefficient  $A_2$ , it is a measure of phase stability, as has been shown for proteins.<sup>16–19</sup> Table S1 in the ESI† gives the values of  $A_2$  for the WLM samples calculated according to eqn (11). For the calculations a mass density  $\rho_{\text{cyl}}$  of  $1.13 \text{ g ml}^{-1}$  and a scattering length density contrast of  $-6.66 \times 10^{10} \text{ cm}^{-2}$  was employed.<sup>26</sup>

The intersection of all lines in Fig. 4 at  $\nu^{a=0}$  and  $\Theta_{s-s}^{a=0}$  can be assigned to the point, where the Coulomb interactions are screened as outlined in the Theory section. When the interactions between micelles are totally screened  $A_2$  is solely determined by excluded volume interactions because the van der Waals parameter  $a \approx 0$  in eqn (1). According to eqn (1)–(3), the term  $b/M^2$  is constant for worm-like chains with a constant radius. The relations can be employed to calculate a theoretical  $\nu^{a=0}$ . Bearing in mind that for WLMs the molar mass  $M = N_A \pi R^2 L_2 \rho_{\text{cyl}}$  and  $V^{\text{mf}} = 1/2 N_A \pi R L_2^2$ , eqn (2) can be restated,

$$A_2(a=0) = \frac{V^{\text{mf}}}{M^2} = \frac{1}{2 N_A \pi R^3 \rho_{\text{cyl}}^2} \quad (16)$$

The radius of the mixed surfactant WLMs is on average  $17.6 \text{ \AA}$ . Employing eqn (11) and (16), a theoretical value of  $\nu^{a=0} \approx 0.013 \text{ cm}$  is obtained. This value is about 40% lower than the experimentally

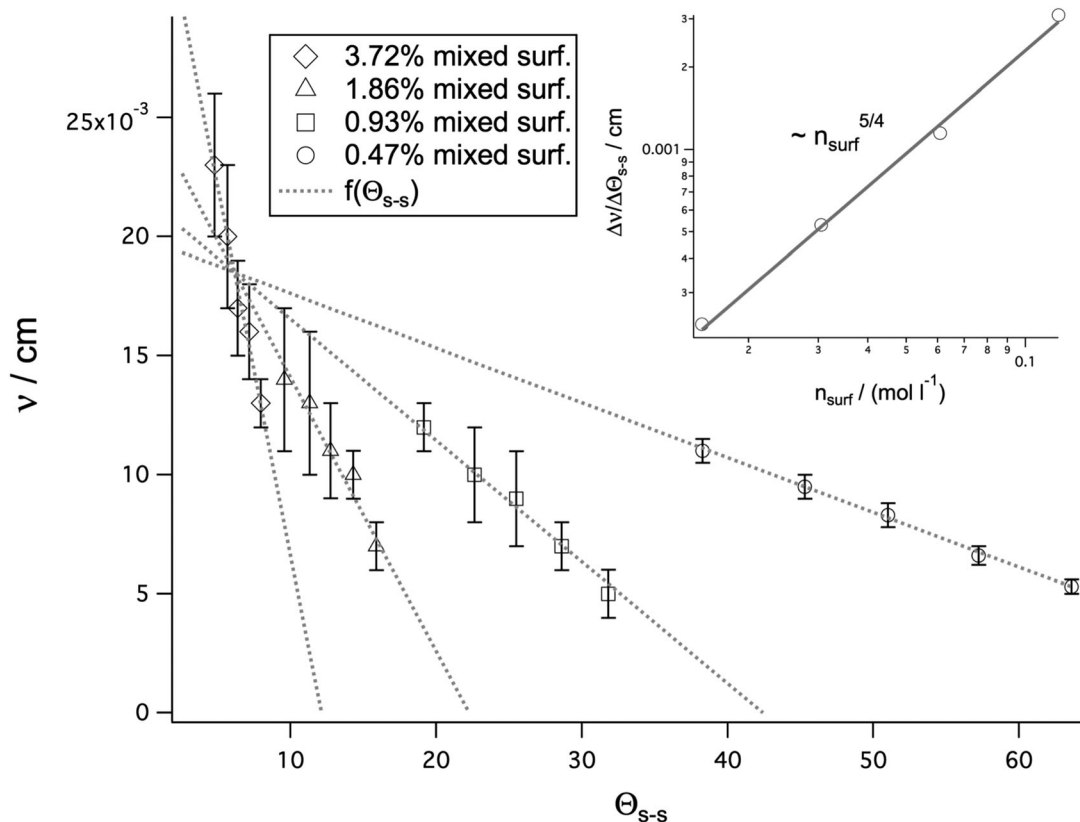


Fig. 4 Screening parameter  $\nu$  vs. salt-surfactant ratio  $\Theta_{s-s}$ . The dashed lines denote a linear relation of the form  $f(\Theta_{s-s}) = 0.0185 \text{ cm} - (\Delta\nu/\Delta\Theta_{s-s})(\Theta_{s-s} - 6.16)$ . The inset depicts a plot of  $\log(\Delta\nu/\Delta\Theta_{s-s})$  vs.  $\log(n_{\text{surf}})$ , where  $n_{\text{surf}}$  is the mixed surfactant concentration in  $\text{mol l}^{-1}$ .

observed value. A possible explanation for this deviation might be that  $f = L/(2R)$  is strictly valid for stiff cylinders. WLMs, however, are flexible and tortuous structures. While the presence of the predicted intersection of  $\nu$  values in Fig. 5 suggests that the contour length dependence cancels for stiff or flexible

cylinders, deviations in the exact value of  $f$  due to chain flexibility might explain the difference between the observed and theoretically predicted intersection point given that for the calculation of the theoretical  $\nu^{\alpha=0}$  the WLMs were hypothesized as rigid bodies and the impact of polydispersity was ignored. Eqn (16) just serves as a first-order approximation for a polydisperse soft-matter system like WLMs.

Below  $\Theta_{s-s}^{\alpha=0}$  the interactions between WLM segments are repulsive due to Coulombic interactions. Above  $\Theta_{s-s}^{\alpha=0}$ , through most of the studied range, the interactions between WLM segments are attractive and the solutions remain single phase solely due to exclude volume as will be discussed in the next section.

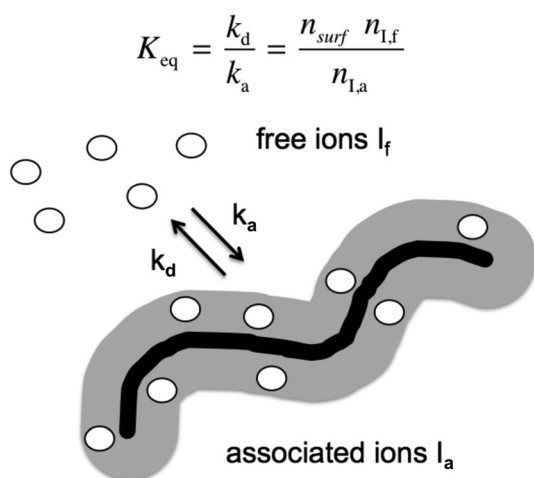


Fig. 5 Sketch of the equilibrium between free ions in solution and ions associated with the ion cloud surrounding the WLM. The ion-cloud model predicts an equilibrium between free ions,  $n_{\text{I,f}}$ , and ions associated with the WLM in an ion cloud,  $n_{\text{I,a}}$ . The concentration of surfactant molecules,  $n_{\text{surf}}$ , governs the area of the ion cloud.

#### A microscopic interpretation of the screening parameter $\nu$

Long WLMs usually assemble at relatively high salt concentrations *i.e.*, under strong screening of charges. Such conditions necessarily imply that interactions are restricted to short range. As seen in the previous section, these interactions can become attractive. Thus, a microscopic interpretation has to explain how interactions restricted to short range between particles carrying the same charge can gradually change from repulsive regime to attractive upon addition of salt.

Since the WLMs must be close to each other to interact, the salt ions in the interspace can be envisioned as confined between two or more charged surfaces. Two charged surfaces separated by an electrolyte solution can give rise to the formation

of an ion cloud.<sup>37</sup> Under certain conditions fluctuations in the cloud around the charged layers can lead to net attractive interactions between similarly charged surfaces.

The concept of an ion cloud surrounding charged WLMs can account for the occurrence of attractive interactions between particles bearing the same charge type in analogy to van der Waals interactions. Fluctuations of charge within the cloud lead to both attraction and repulsion with equal probability; however, the Coulombic force depends on  $1/R^2$  where  $R$  is the separation distance. So an attractive potential has a larger contribution to the net force since  $R$  is slightly smaller as the particles are attracted.

Interactions between WLM subunits can be modeled using an association/dissociation equilibrium between free ions in solution and an ion cloud surrounding the WLM. Introducing the symbol “S” for the surfactant species and “I” for the ion, the following equilibrium reaction can be formulated.



where  $I_f$  represents the free ions in solution and  $I_a$  those associated with the cloud surrounding the WLM surface. The parameters  $k_a$  and  $k_d$  are the reaction's association and dissociation constants, respectively. The association of ions and their partial immobilization is the result of their spatial vicinity to the charged WLM surface, here represented by the surfactant species S. The spatial vicinity between the associated ion  $I_a$  in the ion cloud and the WLM is expressed *via* the rectangular brackets on the right hand side of the reaction equation.

The sum of the concentration of the free ions  $n_{I,f}$  plus the associated ions  $n_{I,a}$  yields the total concentration of ions  $n_{I,0}$ .

$$n_{I,0} = n_{I,f} + n_{I,a} \quad (18)$$

Note that the symbol I for the ionic species rather than concretely  $\text{Na}^+$  or  $\text{Cl}^-$  is employed here to allow ambiguity. Present data in the form of the salt-surfactant ratio  $\Theta_{ss}$  does not distinguish between anions and cations. It cannot be taken for granted that just counterions like  $\text{Na}^+$  will associate in the ion cloud. The cloud may not be spatially uniform and both anions as well as cations may be involved in its assembly. The question whether just the cations or both ionic species take part in the association/dissociation reaction has to be left open at this point. Fig. 5 depicts a sketch of this equilibrium reaction.

Basing on eqn (17) the following change of  $n_{I,f}$  with time  $t$  can be described.

$$\frac{dn_{I,f}}{dt} = -k_a n_{I,f} n_{\text{surf}} + k_d n_{I,a} \quad (19)$$

Note that the association term for  $d(n_{I,f})/(dt)$  depends on the total surfactant concentration  $n_{\text{surf}}$ , because the number of association “sites” within the cloud is not limited to a distinct number, but scales with the area of the charged surface and is proportional to  $n_{\text{surf}}$ . Accordingly, dissociation only depends on the concentration of associated ions  $n_{I,a}$ .

In equilibrium  $dn_{I,f}/dt = 0$ , and the equilibrium constant  $K_{\text{eq}}$  can be formulated.

$$K_{\text{eq}} = \frac{k_d}{k_a} = \frac{n_{I,f} n_{\text{surf}}}{n_{I,a}} \quad (20)$$

Rearrangement and expansion with  $n_{\text{surf}}$  yields,

$$\frac{n_{I,a}}{n_{\text{surf}}} = \frac{n_{\text{surf}}}{K_{\text{eq}}} \left( \frac{n_{I,0}}{n_{\text{surf}}} - \frac{n_{I,a}}{n_{\text{surf}}} \right) = \frac{n_{\text{surf}}}{K_{\text{eq}}} \left( \Theta_{s-s} - \frac{n_{I,a}}{n_{\text{surf}}} \right) \quad (21)$$

since  $n_{I,f} = n_{I,0} - n_{I,a}$  and  $n_{I,0}/n_{\text{surf}} = \Theta_{s-s}$ . Rearranging eqn (21),

$$\frac{n_{I,a}}{n_{\text{surf}}} = \frac{\Theta_{s-s}}{\frac{K_{\text{eq}}}{n_{\text{surf}}} + 1} \quad (22)$$

Abbreviating the ratio of associated ion concentration over the total surfactant concentration  $n_{I,a}/n_{\text{surf}}$  as  $\Theta_a$  and assuming that the ratio  $K_{\text{eq}}/n_{\text{surf}} \gg 1$ , or  $n_{I,f}/n_{I,a} \gg 1$  from eqn (20), the expression simplifies to

$$\Theta_a \approx \frac{n_{\text{surf}}}{K_{\text{eq}}} \Theta_{s-s} \quad (23)$$

In this limit the ratio of associated ions to surfactant is proportional to the overall salt-surfactant ratio  $\Theta_{s-s}$ . It is hypothesized that there is a certain ratio of associated ions over total surfactant  $\Theta_a = \Theta_a^{a=0}$ , where Coulombic interactions between the WLMs cancel out resulting in  $\nu = \nu^{a=0}$  (see Fig. 4). The lower index “a” signifies that the ratio of the associated ions to the cloud is considered, while the upper index “a = 0” refers to the point  $\nu^{a=0}$ , where all values of  $\nu$  intersect. Accordingly the symbol  $\Theta_{s-s}^{a=0}$  refers to the overall salt-surfactant ratio where  $\nu = \nu^{a=0}$ . The offset ratio  $\Theta_a^{a=0}$  of bound ions applied to the left side of eqn (23) corresponds to a  $\Theta_{s-s}^{a=0}$  serving as an offset for  $\Theta_{s-s}$  on the right hand side.

$$\Theta_a - \Theta_a^{a=0} = \frac{n_{\text{surf}}}{K_{\text{eq}}} (\Theta_{s-s} - \Theta_{s-s}^{a=0}) \quad (24)$$

Repulsive forces between micelles, and concomitantly  $A_2$ , and  $\nu$ , decrease with increasing  $\Theta_{s-s}$  due to Debye screening. Eqn (23) indicates that  $\Theta_{s-s}$  is proportional to  $\Theta_a$ . At  $\nu = \nu^{a=0}$ , corresponding to  $\Theta_{s-s}^{a=0} \propto \Theta_a^{a=0}$ , the interactions change from repulsive to attractive. Assuming proportionality between  $A_2$  and  $\Theta_a$ ,

$$\nu = \nu^{a=0} [1 - (\Theta_a - \Theta_a^{a=0})] \quad (25)$$

An expansion of eqn (24) according to (25) yields

$$\nu = \nu^{a=0} \left[ 1 - \frac{n_{\text{surf}}}{K_{\text{eq}}} (\Theta_{s-s} - \Theta_{s-s}^{a=0}) \right] \quad (26)$$

in agreement with eqn (15). The exponent of 5/4 applied in latter formula to the ratio of  $(n_{\text{surf}}/K_{\text{eq}})$  could be considered an empirical correction. On the other hand, scaling laws for wormlike systems demonstrate the necessity for this behavior in the semi-dilute regime for good solvents.<sup>6,10</sup> If eqn (15) is valid, as substantiated above, a plot according to

$$\frac{\nu - \nu^{a=0}}{\nu^{a=0}} \left( \frac{K_{\text{eq}}}{n_{\text{surf}}} \right)^3 = (\Theta_{s-s} - \Theta_{s-s}^{a=0}) \quad (27)$$

should yield a straight line. Fig. 6 depicts such a plot and demonstrates that this is indeed the case.

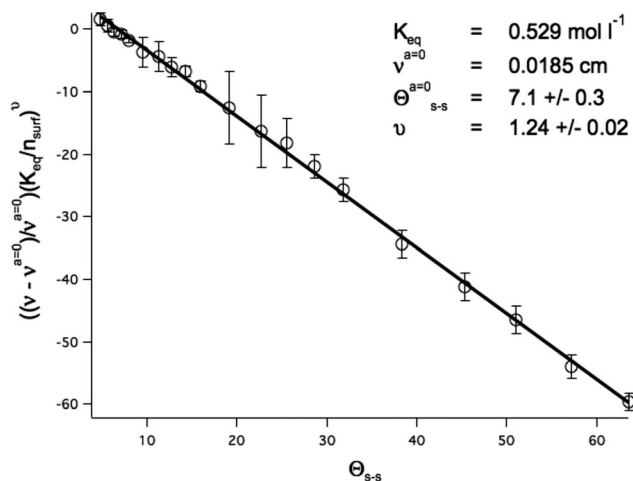


Fig. 6 Verification of the ion-cloud, association/dissociation model. Plot shows the reduced second virial coefficient as a function of salt–surfactant ratio as described by eqn (27).

Eqn (27) can be reformulated for the second virial coefficient using eqn (2) and (11),

$$A_2 = \frac{b}{M^2} \left[ 1 - \frac{n_{\text{surf}}}{K_{\text{eq}}} (\Theta_{s-s} - \Theta_{s-s}^{a=0}) \right]. \quad (28)$$

With eqn (17)–(27) an interpretation for the observed results in the previous section has been found. The parameter  $\nu$ , observed as the screening of scattering at low  $q$ , can be directly connected to the van der Waals parameters  $b$  and  $a$  via eqn (15) and (26). The  $\Theta_{s-s}$ -independent terms correspond to the excluded volume,  $b$ , as defined in eqn (1) and (2). The  $\Theta_{s-s}$ -dependent part represents the van der Waals parameter  $a$ , as a function of salt concentration. The temperature dependence according to eqn (1) will be the topic of further investigation.

For gases a knowledge of the van der Waals parameters  $a$  and  $b$  allows calculation of the gas–liquid phase boundary via the Maxwell construction, hence the present findings have interesting implications for WLM systems. If the molar mass  $M$  of the WLMs is known (see eqn (1)), the van der Waals parameters  $a$  and  $b$  can be calculated and the phase boundaries can be determined in a similar manner. The molar mass of WLMs is proportional to the contour length  $L_2$ , and methods as depicted in the present work or employing the scission energy  $E_{\text{sc}}^{38}$  can thus serve to calculate phase separation limits for this colloidal system. The derived formulas connect the structure of WLMs with the van der Waals equation of state. Notably, relation (16) allows an estimation of the radius  $R$  for charged wormlike chains via routine scattering techniques like small-angle light scattering. In combination with measurement of the osmotic pressure  $\Pi \approx RT(c_{\text{m}}/M + c_{\text{m}}^2 A_2)$  the contour length  $L_2 \propto M$  can be assessed.

## Conclusion

Self-assembled, thread-like micelles display thermodynamic similarities to macromolecules and to colloids. In both polymers and colloids a virial approach has proven useful to describe

phase behavior. In “living” WLMs the molar mass is dependent on parameters that influence phase stability. Further, formation of worm-like micelles occurs at extremely high salt-to-surfactant ratios that necessitate an ion-cloud model to describe dependencies of the second virial coefficient. This model is verified through neutron scattering measurements.

It is demonstrated that structural screening, and the associated virial coefficient, has an impact on scattering at concentrations above 0.45 wt% surfactant. For this reason scattering studies for WLMs should generally include the RPA-virial approach, especially if the chain contour length is of interest.

It is demonstrated that the second virial coefficient,  $A_2$ , decreases with salt to surfactant ratio consistent with Debye screening of charge. An ion-cloud, association–dissociation, equilibrium model is proposed and verified. This model is coupled with the van der Waals equation of state to split  $A_2$  into a contribution due to the excluded volume and a contribution due to particle–particle interaction. Both contributions are identified and quantitatively described for the WLM system. The interactions are moreover described within the ion-cloud equilibrium model for association and dissociation of salt ions.

## Acknowledgements

This research used resources at the High Flux Isotope Reactor and the Spallation Neutron Source, DOE Office of Science User Facilities operated by the Oak Ridge National Laboratory.

## References

- 1 C. A. Dreiss, *Soft Matter*, 2007, **3**, 956–970.
- 2 E. Sabadini, R. F. S. Ungarato and P. B. Miranda, *Langmuir*, 2014, **30**, 727–732.
- 3 A. L. Fogelson and J. P. Keener, *Phys. Rev. E: Stat., Nonlinear, Soft Matter Phys.*, 2010, **81**, 051922.
- 4 A. S. Wolberg, *Blood Rev.*, 2007, **21**, 131–142.
- 5 C. Bustamante, *Science*, 1994, **256**, 1599–1600.
- 6 I. Noda, N. Kato, T. Kitano and M. Nagasawa, *Macromolecules*, 1981, **14**, 668–676.
- 7 J. des Cloizeaux, *J. Phys.*, 1975, **36**, 281–291.
- 8 M. Daoud, J. P. Cotton, B. Farnoux, G. Jannink, G. Sarma, H. Benoit, C. Duplessix, C. Picot and P.-G. de Gennes, *Macromolecules*, 1975, **8**, 804–818.
- 9 P.-G. de Gennes, *Scaling concepts in polymer physics*, Cornell University Press, Ithaca, N.Y., U.S.A., 1979.
- 10 G. Strobl, *The physics of polymers: Concepts for understanding their structure and behavior*, Springer Verlag, Berlin-Heidelberg, 2007, p. 39 and 87.
- 11 R. H. Colby, *Rheol. Acta*, 2010, **49**, 425–442.
- 12 M. Doi and F. S. Edwards, *The theory of polymer dynamics*, Clarendon Press, New York, Oxford (Oxfordshire), 1986.
- 13 R. Larson, *The structure and rheology of complex fluids*, Oxford University Press, New York, 1999, p. 151.

- 14 J. S. Pedersen and C. Sommer, *Prog. Colloid Polym. Sci.*, 2005, **130**, 70–78.
- 15 T. A. Orofino and P. J. Flory, *J. Chem. Phys.*, 1957, **26**, 1067–1076.
- 16 F. Bonneté, S. Finet and A. Tardieu, *J. Cryst. Growth*, 1999, **196**, 403–414.
- 17 B. L. Neal, D. Asthagiri, O. D. Velez, A. M. Lenhoff and E. W. Kaler, *J. Cryst. Growth*, 1999, **196**, 377–387.
- 18 B. L. Neal, D. Asthagiri and A. M. Lenhoff, *Biophys. J.*, 1998, **75**, 2469–2477.
- 19 J. G. S. Ho, A. P. J. Middelberg, P. Ramage and H. P. Kocher, *Protein Sci.*, 2003, **12**, 708–716.
- 20 T. M. Birshtein, A. M. Skvortsov and A. A. Sariban, *Macromolecules*, 1976, **9**, 892–895.
- 21 P. A. Hassan, S. R. Raghavan and E. W. Kaler, *Langmuir*, 2002, **18**, 2543–2548.
- 22 P. Meakin, I. Majid, S. Havlin and H. E. Stanley, *J. Phys. A: Math. Gen.*, 1984, **17**, L975–L981.
- 23 S. Havlin and R. Nossal, *J. Phys. A: Math. Gen.*, 1984, **17**, L427–L432.
- 24 G. Beaucage, *Phys. Rev. E: Stat., Nonlinear, Soft Matter Phys.*, 2004, **70**, 031401.
- 25 G. Beaucage, *J. Appl. Crystallogr.*, 1995, **28**, 717–728.
- 26 K. Vogtt, G. Beaucage, M. Weaver and H. Jiang, *Langmuir*, 2015, **30**, 8228–8234.
- 27 H. Fujita, *Polymer solutions*, Elsevier Science Publishers B.V., Amsterdam, The Netherlands, 1990, pp. 195–197.
- 28 P. W. Anderson, *Phys. Rev.*, 1958, **112**, 1900–1916.
- 29 J. S. Pedersen and P. Schurtenberger, *Europhys. Lett.*, 1999, **45**, 666–672.
- 30 W. W. Graessley, *Macromolecules*, 2002, **35**, 3184–3188.
- 31 B. H. Zimm, *J. Chem. Phys.*, 1948, **16**, 1093–1099.
- 32 H. Benoit and M. Benmouna, *Polymer*, 1984, **25**, 1059–1067.
- 33 J. S. Pedersen, *Adv. Colloid Interface Sci.*, 1997, **70**, 171–210.
- 34 R. S. Stein and G. Hadziioannou, *Macromolecules*, 1984, **17**, 1059–1062.
- 35 A. Guinier and G. Fournet, *Small-angle scattering of x-rays*, John Wiley & Sons, New York, 1955, p. 48.
- 36 R. Ramachandran, G. Beaucage, A. Kulkarni, D. McFaddin, J. Merrick-Mack and V. Galiatsatos, *Macromolecules*, 2009, **42**, 4746–4750.
- 37 L. Guldbrand, B. Jönsson, H. Wennerström and P. Linse, *J. Chem. Phys.*, 1984, **80**, 2221–2228.
- 38 I. Couillet, T. Hughes, G. Maitland, F. Candau and S. J. Candau, *Langmuir*, 2004, **20**, 9541–9550.